Clim. Past, 7, 1041–1059, 2011
www.clim-past.net/7/1041/2011/
doi:10.5194/cp-7-1041-2011

Climate of the Past

Sensitivity of interglacial Greenland temperature and $\delta^{18}O$: ice core data, orbital and increased CO_2 climate simulations

V. Masson-Delmotte[1], P. Braconnot[1], G. Hoffmann[1], J. Jouzel[1], M. Kageyama[1], A. Landais[1], Q. Lejeune[1], C. Risi[2], L. Sime[3], J. Sjolte[4], D. Swingedouw[1], and B. Vinther[4]

[1]Laboratoire des Sciences du Climat et de l'Environnement, UMR8212, CEA-CNRS-UVS, Gif-sur-Yvette, France
[2]CIRES, U. Colorado, Boulder, USA
[3]British Antarctic Survey, Cambridge, UK
[4]Centre for Ice and Climate, Niels Bohr Institute, University of Copenhagen, Copenhagen, Denmark

Received: 17 May 2011 – Published in Clim. Past Discuss.: 23 May 2011
Revised: 2 September 2011 – Accepted: 2 September 2011 – Published: 29 September 2011

Abstract. The sensitivity of interglacial Greenland temperature to orbital and CO_2 forcing is investigated using the NorthGRIP ice core data and coupled ocean-atmosphere IPSL-CM4 model simulations. These simulations were conducted in response to different interglacial orbital configurations, and to increased CO_2 concentrations. These different forcings cause very distinct simulated seasonal and latitudinal temperature and water cycle changes, limiting the analogies between the last interglacial and future climate. However, the IPSL-CM4 model shows similar magnitudes of Arctic summer warming and climate feedbacks in response to $2 \times CO_2$ and orbital forcing of the last interglacial period (126 000 years ago).

The IPSL-CM4 model produces a remarkably linear relationship between TOA incoming summer solar radiation and simulated changes in summer and annual mean central Greenland temperature. This contrasts with the stable isotope record from the Greenland ice cores, showing a multi-millennial lagged response to summer insolation. During the early part of interglacials, the observed lags may be explained by ice sheet-ocean feedbacks linked with changes in ice sheet elevation and the impact of meltwater on ocean circulation, as investigated with sensitivity studies.

A quantitative comparison between ice core data and climate simulations requires stability of the stable isotope – temperature relationship to be explored. Atmospheric simulations including water stable isotopes have been conducted with the LMDZiso model under different boundary conditions. This set of simulations allows calculation of a temporal Greenland isotope-temperature slope (0.3–0.4 ‰ per °C) during warmer-than-present Arctic climates, in response to increased CO_2, increased ocean temperature and orbital forcing. This temporal slope appears half as large as the modern spatial gradient and is consistent with other ice core estimates. It may, however, be model-dependent, as indicated by preliminary comparison with other models. This suggests that further simulations and detailed inter-model comparisons are also likely to be of benefit.

Comparisons with Greenland ice core stable isotope data reveals that IPSL-CM4/LMDZiso simulations strongly underestimate the amplitude of the ice core signal during the last interglacial, which could reach +8–10 °C at fixed-elevation. While the model-data mismatch may result from missing positive feedbacks (e.g. vegetation), it could also be explained by a reduced elevation of the central Greenland ice sheet surface by 300–400 m.

Correspondence to:
V. Masson-Delmotte
(valerie.masson@cea.fr)

1 Introduction

Greenland ice cores, such as the longest NorthGRIP record, spanning the last 123 000 years (NorthGRIP-community-members, 2004), offer continuous and quantitative archives of past local climate variability at orbital time scales (e.g. Vinther et al., 2009) as well as the evidence for abrupt climate events (e.g. Capron et al., 2010a). Ice core data allow us to explore the past magnitudes and rates of changes of central Greenland temperature prior to the instrumental period (Masson-Delmotte et al., 2006a), even with uncertainties related to the conversion of ice core proxies into past temperatures, to the age scales, and to the glaciological processes (Vinther et al., 2009).

Published by Copernicus Publications on behalf of the European Geosciences Union.

In principle, these data can provide a benchmark to test the ability of climate models to correctly represent climate feedbacks (Otto-Bliesner et al., 2006). Past changes in orbital forcing indeed provide natural externally forced experiments on the Earth's climate, leading to past interglacial periods with Arctic temperatures warmer than present-day and large changes in Greenland ice sheet volume (Kopp et al., 2009; Vinther et al., 2009). In particular, the last interglacial period, about 130–120 thousand years before present (ka), is proposed to be a good analogue for future climate change driven by anthropogenic greenhouse gas emissions (Clark and Huybers, 2009; Otto-Bliesner et al., 2006; Sime et al., 2009; Turney and Jones, 2010), especially in the Arctic.

In this manuscript, we address the following questions:

- What is the Greenland ice core quantitative information on past surface temperature changes during the current and last interglacial, and how is it related to orbital forcing? This requires the relationship between Greenland surface temperature and snowfall isotopic composition, and the various processes that can modify this relationship through time, to be understood.

- Which changes in Greenland climate are produced by an ocean-atmosphere model in response to different interglacial orbital configurations? For this purpose, we analyze long snapshot simulations conducted with the IPSL-CM4 model forced only by the orbital configuration of key periods of the current and last interglacial at 0, 6, 9.5, 115 and 126 ka. For 126 ka, we also consider a sensitivity test to a simple parameterization of Greenland ice sheet melt allowing representation of the impact of meltwater on the ocean circulation (Swingedouw et al., 2009).

- What are the analogies and differences between the climate response to the forcings associated with increased CO_2 concentrations and to changes in orbital configuration? For this purpose, we compare the IPSL-CM4 response to higher atmospheric CO_2 concentrations and to the last interglacial insolation change, with a focus on Greenland climate. Indeed, climate projections ($2\times$ and $4\times CO_2$) give access to climate states with 3 to 8 °C warmer central Greenland annual mean temperature (Masson-Delmotte et al., 2006b).

- Is the climate model able to capture the magnitude of changes derived from the ice core data? For direct model-data comparisons, we use the sea surface conditions (sea surface temperature, SST and sea ice) from the coupled climate model to drive its atmospheric component equipped with the explicit modeling of precipitation isotopic composition (LMDZiso). This also allows the stability of the isotope-temperature change through time and the mechanisms that can alter this relationship to be explored.

- What was the change in central Greenland ice sheet topography during the last interglacial? The IPSL-CM4 and LMDZiso simulations appear to underestimate the magnitude of last interglacial temperature and precipitation isotopic composition changes compared to the Greenland ice core data. Assuming that the model-data mismatch is mainly caused by a reduced ice sheet elevation, we can estimate the magnitude of this elevation change.

In order to address these questions, Sect. 2 is dedicated to the information obtained from the NorthGRIP ice core. Section 3 describes the results of the IPSL-CM4 coupled ocean-atmosphere model climate under different orbital configurations. The response of the central Greenland climate to orbital forcing is also compared to its response to projections of higher greenhouse gas concentrations. An analysis of the key radiative feedbacks affecting the top of the atmosphere radiative budget is proposed. In Sect. 4, we investigate the Greenland isotope-temperature relationship for warmer-than-present climates using isotopic atmospheric general circulation models (LMDZiso and HadAM3iso) and discuss the implications for past central Greenland temperature and possible elevation changes.

2 Ice core information on past Greenland temperature

2.1 Water stable isotopes – climate relationships

Continuous records of water stable isotopes ($\delta^{18}O$ or δD) have been measured along several deep Greenland ice cores; the longest record published so far was obtained from the NorthGRIP ice core (NorthGRIP-community-members, 2004) (Fig. 1). The initial vapour is formed by evaporation at the ocean surface. Its isotopic composition is affected by evaporation conditions through equilibrium and kinetic fractionation processes, and it depends on moisture sources temperature and relative humidity. Along the air mass trajectories to Greenland, the isotopic composition of the atmospheric water vapour undergoes mixing by convection, upload of new water vapor from different sources, and distillation linked with the progressive air mass cooling and successive condensation, as well as kinetic effects on ice crystals. Altogether, these physical processes result in a linear relationship between the air temperature and the snowfall isotopic composition in central Greenland. For $\delta^{18}O$, the slope of the modern spatial relationship is 0.7 ‰ per °C for the first ice core sites (e.g. Dye 3, Camp Century) (Dansgaard, 1964), and 0.8 ‰ per °C for all available data including coastal stations (Dansgaard, 1964; Sjolte et al, 2011).

In addition to the impact of condensation temperature, several effects can affect the precipitation isotopic composition and modify the temporal isotope-temperature relationship

- *deposition effects*, caused by precipitation intermittency or changes in the relationship between the temperature

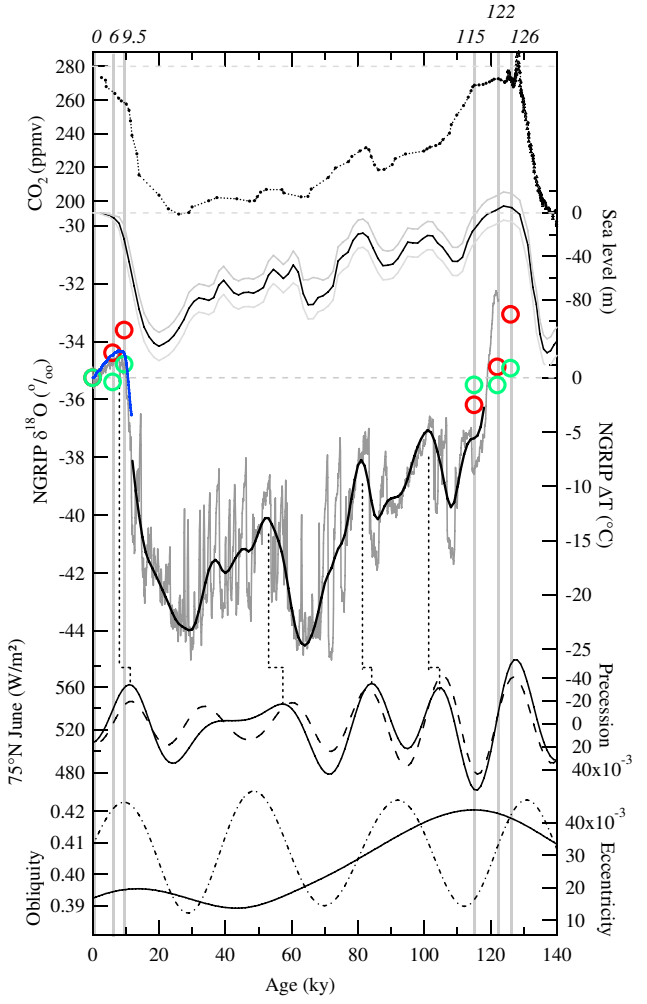

Fig. 1. From top to bottom: black dots, atmospheric CO_2 concentration (Vostok and EDC ice cores) on the EDC3 age scale (Barnola et al., 1987; Lourantou et al., 2010); solid black line with uncertainties, estimation of eustatic sea level (Waelbroeck et al., 2002); NorthGRIP ice core δ^{18}O data on a 20 year resolution on GICC05 and EDC3 age scale (Capron et al., 2010a). The orbital component of the record is displayed (thick black line) and was calculated using the first three components of a singular spectrum analysis. A tentative estimate of the temperature change is also displayed, following Masson-Delmotte et al. (2005b) (right axis). The reconstruction of the Holocene Greenland temperature (at fixed elevation) (Vinther et al., 2009) is displayed as a bold blue line. Summer (red) and annual mean (green) temperature anomalies simulated by the IPSL model are displayed as open circles for 6, 9.5, 115, 122, and 126 ka. The 75° N June insolation (black line, W m^{-2}) and orbital parameters (precession parameter – long dashed line, obliquity – short dashed line, and eccentricity – solid black line) are displayed in the two lowest panels.

at the condensation level and the surface temperature (Jouzel et al., 1997). Modern observations suggest greater summer than winter precipitation in central Greenland (Shuman et al., 1995), which differs from deposition seasonality in Antarctica (Laepple et al., 2011). Atmospheric models have shown a large deposition effect for Greenland glacial climate, due to strongly reduced winter precipitation (Krinner et al., 1997; Werner et al., 2000). In this manuscript, we assess the "precipitation-weighting effect" by comparing the average temperature change to the monthly precipitation-weighted temperature change;

– *source effects*, caused by changes in evaporation conditions or moisture origin (Johnsen et al., 1989; Jouzel et al., 2007; Masson-Delmotte et al., 2005a,c);

– *glaciological effects*, caused by changes in ice sheet topography which affects surface air temperature and stable isotopic composition (Vinther et al., 2009). We therefore introduce the notion of temperature estimate "at fixed elevation", by contrast with the information on air temperature at the ice sheet surface classically derived from stable isotope data (Masson-Delmotte et al., 2005a).

Alternative information on past Greenland temperature is available from the borehole temperature profiles (Dahl-Jensen et al., 1998) and from firn gas fractionation during abrupt warmings (Capron et al., 2010a; Severinghaus et al., 1998). The latter method allows the estimation of the interstadial isotope-temperature slope to range between 0.30 ± 0.05 and 0.60 ± 0.05 ‰ of δ^{18}O per °C (Capron et al., 2010a), therefore quite different from the spatial slope. This likely results from deposition and source effects (Masson-Delmotte et al., 2005a). In Sect. 4, we will use isotopic simulations to quantify the isotope-temperature relationship in warmer-than-present climate conditions.

2.2 Greenland Holocene climate and ice sheet elevation

Recently, Vinther et al. (2009) conducted a synthesis of the Greenland ice core Holocene stable isotope information. It combines ice core records from coastal ice caps (where changes in elevation are limited) and from the central ice sheet (where higher elevation changes can significantly affect the isotopic signals). The authors extract a common and homogeneous annual mean Greenland temperature signal "at fixed elevation", together with regional changes in the ice sheet topography. The new "fixed elevation" temperature history from this study (Fig. 1, central panel, blue line) reveals a pronounced Holocene climatic optimum in Greenland coinciding with a maximum thinning near the ice sheet margins. These results also imply that the NorthGRIP ice core δ^{18}O data can be converted to temperature with a temporal slope of 0.45 ‰ per °C.

They calculate that the elevation of the NorthGRIP site has decreased by ~140 m since 9.5 kyr and by ~60 m from 6 ka to present. The central Greenland temperature "at fixed elevation" is estimated to be ~2.3 °C higher at 9.5 ka and ~2.0 °C at 6 ka than during the last millennium, with a multi-millennial warm plateau encountered between 9.3 and 6.8 ka.

This plateau occurs 1.8 to 4.3 kyr (thousand years) later than the maximum in 75° N June insolation. The early Holocene warmth is partly masked in the central Greenland ice core stable isotope records because of the larger volume and elevation of the ice sheet.

2.3 Links between NorthGRIP δ^{18}O and 75° N summer insolation

We extract the orbital components of the NorthGRIP record using the first components of a Singular Spectrum Analysis performed on the whole series and corresponding to periodicities longer than 3 kyr (Fig. 1, bold line, central panel). With the available ice core age scales (Capron et al., 2010b; Svensson et al., 2008), the orbital component of the NorthGRIP δ^{18}O appears to lag the reversed precession parameter (in phase with local June insolation) by several millennia (Fig. 1). A significant correlation ($R^2 = 0.27$) is obtained between the smoothed NorthGRIP δ^{18}O and 4 kyr earlier 75° N June insolation. The four most recent optima in this smoothed NorthGRIP δ^{18}O record lag maxima in 75° N June insolation by 4.8, 4.8, 3.1 and 3.5 kyr, respectively (Fig. 1, dashed vertical lines). These lags are significantly larger than the GICC05 (Rasmussen et al., 2006; Svensson et al., 2008)) age scale uncertainty (∼80 years at 10 ka, ∼440 years at 20 ka, ∼1000 years at 30 ka and ∼2600 years at 60 ka) and occur both under glacial and interglacial contexts.

For the Holocene, it is obvious that the Greenland optimum (at ∼7–10 ka) occurs later than the 11 ka precession minimum (local June insolation maximum), likely because of the negative feedback linked with the Laurentide ice sheet albedo and weaker northward advection of heat in the Atlantic Ocean caused by the meltwater from deglaciating Northern Hemisphere ice sheets (Renssen et al., 2009). The NorthGRIP record does not allow this aspect to be explored for the last interglacial because it does not span the whole length of this period (NorthGRIP-community-members, 2004). Marine sediment records of North Atlantic sea surface temperature suggest a pattern similar to the Holocene with a lag between peak insolation and peak isotopic values (Masson-Delmotte et al., 2010a). During the end of the interglacials (after optima in insolation and in δ^{18}O), parallel decreasing trends in 75° N June insolation and NorthGRIP δ^{18}O are observed. For the mid to late Holocene (the last 8 kyr), the δ^{18}O-insolation slope is 0.02 ‰ per W m^{-2} (0.03 to 0.06 °C per W m^{-2}), much weaker than for the end of the last interglacial (121 to 115 ka), where it reaches 0.10 ‰ per W m^{-2} (∼0.17 to 0.33 °C per W m^{-2}).

2.4 Last interglacial Greenland climate

The ice core information on central Greenland climate during the last interglacial is not as precise as for the Holocene due to the age scale uncertainty, the end of the NorthGRIP record at ∼123 ka, and the lack of information from borehole thermometry to constrain the isotope-temperature-elevation histories. Based on the shape of north Atlantic SST records synchronized on the EDC3 age scale (Masson-Delmotte et al., 2010a), one may assume that the isotopic values of the deepest part of the NorthGRIP ice core may be representative of a multi-millennial temperature plateau. Considering the uncertainty on the isotope-temperature relationship (between 0.3 and 0.8 ‰ per °C), the NorthGRIP Last Interglacial ∼3 ‰ δ^{18}O anomaly would translate into a 3.8–10.0 °C surface temperature anomaly. The signal for the last interglacial is without doubt larger than for the early to mid Holocene (see Sect. 2.2), as expected from the larger orbital forcing (Fig. 1).

By themselves, the data do not allow us to quantify the deposition or glaciological effects affecting this temperature estimate, motivating the use of climate models to explore the mechanisms controlling precipitation isotopic composition.

3 Climate modelling

3.1 IPSL-CM4 coupled climate model simulations

The IPSL-CM4 coupled climate model has been extensively used for CMIP3 and PMIP2 simulations (Alkama et al., 2008; Born et al., 2010; Braconnot et al., 2007, 2008; Kageyama et al., 2009; Marti et al., 2010; Swingedouw et al., 2006). The model couples the atmospheric component LMDZ (Hourdin et al., 2006) with the OPA ocean component (Madec and Imbard, 1996). A sea ice model (Fichefet and Maqueda, 1997) which computes the ice thermodynamics and physics is coupled with the ocean-atmosphere model. The ocean and atmosphere exchange momentum, heat and freshwater fluxes, as well as surface temperature and sea ice once a day, using the OASIS coupler (Valcke, 2006). None of the fluxes are corrected or adjusted. The model is run with a horizontal resolution of 96 points in longitude and 71 points in latitude (3.75° × 2.5°) for the atmosphere and 182 points in longitude and 149 points in latitude for the ocean. There are 19 vertical levels in the atmosphere and 31 levels in the ocean, where the highest resolution (10 m) is focused on the upper 150 m. The model reproduces the main features of modern climate, although large temperature or precipitation biases can be partly related to the resolution (Marti et al., 2010). The North Atlantic is often marked by large cold biases in coupled climate models. This is also the case for IPSL-CM4 where a weak Atlantic Meridional Oceanic Circulation (AMOC) (Swingedouw et al., 2007) is linked with a cold bias for central Greenland.

The IPSL-CM4 model results have previously been compared with the ice core information and other model results in terms of polar amplification under glacial conditions or climate projection scenarios (Masson-Delmotte et al., 2006a,b) as well as briefly for the last interglacial (Masson-Delmotte

et al., 2010b). These previous studies showed that the IPSL-CM4 model response is comparable to other climate models and generally seems to underestimate the magnitude of temperature changes compared to those derived from the ice core data.

A set of simulations has been conducted to explore the response of the model to various orbital configurations encountered during the current and last interglacial (see the grey vertical bars in Fig. 1 and the simulation descriptions in Table 1), with all other boundary conditions kept as for the model control simulation (pre-industrial). Small changes in atmospheric composition (CO_2, CH_4) leading to radiative perturbations $<0.4\,W\,m^{-2}$ during the current and last interglacial were neglected, except for the 6 ka simulation following the PMIP2 protocol (Braconnot et al., 2007). The time periods for these simulations (at 0, 6, 9.5, 115, 122 and 126 ka) were chosen to represent contrasting changes in the seasonal cycle of insolation, with different combinations of precession (rather similar at 0 and 115 ka, 122 and 6 ka, 9.5 and 126 ka), obliquity (maximum at 9.5 and minimum at 115 ka) and eccentricity (minimum at 0 ka and maximum at 115 ka) configurations (Braconnot et al., 2008). These simulations were integrated from 300 to 1000 years depending on the time period (Table 1). Since changes in Earth's orbital parameters only marginally affect the global annual mean simulations, these simulations adjust very rapidly to the insolation forcing (50–100 years) from the same initial state. We consider here mean annual cycles computed from 150 to 400 years. Our analysis focuses on the most contrasting simulations, 126 ka and 115 ka. Note that the Antarctic ice core data depict atmospheric CO_2 levels close to the pre-industrial (273–276 ppmv) during these two time periods (Masson-Delmotte et al., 2010a).

We have also used a similar approach to that of Sime et al. (2008) whilst exploring different forms of warmer Greenland climates. We have therefore also analyzed simulations run under projected increased CO_2 concentrations. The $2 \times CO_2$ simulation has been integrated for 250 years. Beginning from a pre-industrial simulation, the atmospheric CO_2 concentration is increased by 1 % per year until it doubles within 70 years (from 280 to 560 ppmv). It is then kept constant for the remaining 180 years. The same protocol is followed for the $4 \times CO_2$ simulation (quadrupling of CO_2 in 140 years and then kept constant for the remaining 110 years). We have used the model outputs averaged over the last 100 years of these simulations.

While the topography of the Greenland and Antarctic ice sheet is constant for all the simulations, a parameterization of Greenland melt has been implemented in order to explore the feedbacks between Greenland warming, Greenland meltwater flux and thermohaline circulation (Swingedouw et al., 2009) with implications for monsoon areas (Braconnot et al., 2008). A simulation including this parameterisation under 126 ka orbital forcing was integrated for 350 years. The thermohaline circulation is affected by an additional freshwater flux and adjusts within 150 years to the forcing. After this adjustment, the deep ocean drift is limited.

3.2 Impact of orbital forcing on IPSL-CM4 simulated central Greenland climate

Figure 2 displays the model results for central Greenland using the same definition as in Masson-Delmotte et al. (2006a), that is the temperature averaged at places where ice sheet elevation is above 1.3 km. For each simulation, monthly mean values of central Greenland temperatures are displayed as a function of monthly mean values of 75° N top of atmosphere (hereafter TOA) incoming solar radiation. The elliptic shape of the plots reflects the one month seasonal lag between surface air temperature and insolation, mostly because of the thermal inertia of the surrounding oceans affecting heat advection to central Greenland. Orbital forcing alone has limited impacts on the simulated winter temperature (because of a weak incoming insolation at that season and latitude) and a strong impact on summer-fall temperatures.

The simulated change in summer temperature is dominating the simulated annual mean temperature change (Table 2). Compared with the pre-industrial control simulation, July (respectively annual mean) temperature changes vary by $-2.5\,°C$ ($-0.5\,°C$) for 115 ka to $+5.8\,°C$ ($+0.9\,°C$) for 126 ka. The model results for summer and annual mean temperature are depicted in Fig. 1 with red and green open circles, respectively. This comparison suggests that the IPSL-CM4 simulation has the right sign of temperature changes, but underestimates the magnitude of annual mean changes compared to the ice core derived information. We now explore the simulated deposition effects, which can impact the model-data comparison, focusing on the precipitation weighting effect.

For all orbital contexts, the IPSL-CM4 model shows a positive precipitation weighting effect (difference between monthly precipitation-weighted temperature and annual mean temperature) (Table 2, last column). This effect is minimum at 115 ka (1.8 °C), maximum at 126 ka (5.2 °C) and is strongly enhanced with increasing local summer insolation. This is due to a strong (non linear) enhancement of summer precipitation for warmer summer temperatures (Table 2). The IPSL-CM4 model therefore points to a large deposition effect, suggesting that the Greenland ice core warms interglacial proxy records such as stable isotopes, but also ^{10}Be (Wagner et al., 2001; Yiou et al., 1997) may be biased towards summer. The simulated changes in precipitation-weighted temperature are intermediate between the summer and annual mean temperature and vary between $-1.1\,°C$ (at 115 ka) and $+3.6\,°C$ (at 126 ka) (Table 2).

In the IPSL-CM4 simulations, the maximum summer temperature change (occurring in July) appears to be strongly linearly related ($R^2 = 0.99$) with maximum 75° N incoming summer insolation (occurring in June), with a slope of $0.08\,°C$ per $W\,m^{-2}$ (Fig. 2b). We first observe that, even considering this largest signal (July temperature), the model

Table 1. Description of the simulations. The LMDZiso simulations were run for 5 years with climatological forcing averaged from the IPSL-CM4 ouputs, and results analysed for the last 3 years of this simulation. AMIP (Atmospheric Modelling Intercomparison Project) boundary conditions are derived from observed SST and sea-ice (1979 to 2007). Atmospheric composition refers to prescribed changes in greenhouse gas concentrations (e.g. CO_2). In the orbital forcing column, e, o and p respectively stand for eccentricity, obliquity (in °), and perihelia-180°.

Name	Orbital forcing	Atmospheric composition	Greenland melt	Ocean surface
IPSL-0 ka	0 ka $e = 0.016$ $o = 23.4$ $p = 102$	pre-industrial	No	Calculated
IPSL-6 ka	6 ka $e = 0.0187$ $o = 24.1$ $p = 0.89$	6 ka	No	Calculated
IPSL-9.5 ka	9.5 ka $e = 0.0194$ $o = 24.2$ $p = 303$	pre-industrial	No	Calculated
IPSL-115 ka	115 ka $e = 0.0414$ $o = 22.4$ $p = 111$	pre-industrial	No	Calculated
IPSL-122 ka	122 ka $e = 0.0407$ $o = 23.2$ $p = 356$	pre-industrial	No	calculated
IPSL-126 ka	126 ka $e = 0.0397$ $o = 23.9$ $p = 291$	pre-industrial	No	calculated
IPSL-126 ka GM	126 ka	pre-industrial	Yes	calculated
IPSL-2 × CO_2	0 ka	CMIP3	No	Calculated
IPSL-4 × CO_2	0 ka	CMIP3	No	calculated
LMDZiso-ctrl	0 ka	348 ppmv	No	Prescribed from AMIP
LMDZiso-6ky	6 ka	280 ppmv	No	Prescribed as AMIP + (IPSL6 kyr − IPSL0 kyr)
LMDZiso-126 kyr	126 ka	280 ppmv	No	Prescribed as AMIP + (IPSL126 kyr − IPSL0 kyr)
LMDZiso-126 kyr GM	126 ka	280 ppmv	Prescribed from IPSL-126 kyr GM	Prescribed as AMIP + (IPSL126 kyr GM −IPSL0 kyr)
LMDZisoSST	0 ka	280 ppmv	No	AMIP + 4 °C
LMDZiso2 × CO_2	0 ka	2 × 348 ppmv	No	IPSL2 × CO_2
LMDZiso4x × CO_2	0 ka	4 × 348 ppmv	No	IPSL 4 × CO_2

response to summer insolation therefore appears at least half as large as that derived from the ice core data for the transition from 122 to 115 ka (0.17 to 0.33 °C per W m^{-2}, see Sect. 2.3). In Sect. 3.2, we investigate the changes affecting the top of the atmosphere radiative budget and key radiative feedbacks in order to better describe the processes responsible for such a linear model response to the orbital forcing.

Table 2. IPSL-CM4 results for Greenland (from grid points located above 1300 m elevation): annual mean, July and precipitation-weighted temperature (°C) as well as deposition effect (difference between precipitation-weighted and annual mean temperature) and ratio of summer (April–September) to annual precipitation. Results are given for the different simulations in response to orbital forcing only. Absolute values are given as well as anomalies with respect to the control simulation (numbers shown between parentheses).

Simulation	Annual mean Greenland temperature (anomaly) (°C)	July Greenland temperature (anomaly) (°C)	Ratio of summer half year (April–September) to annual precipitation (percentage of change)	Precipitation weighted Greenland temperature (anomaly) (°C)	Deposition effect (anomaly) (°C)
Control simulation	−28.3	−12.9	0.60	−25.9	2.4
6 ka	−27.9 (+0.4)	−10.6 (+2.3)	0.62 (+3 %)	−24.7 (+1.2)	3.2 (+0.7)
9.5 ka	−27.5 (+0.8)	−8.5 (+4.4)	0.65 (+8 %)	−23.3 (+2.6)	4.2 (+1.8)
115 ka	−28.8 (−0.5)	−15.4 (−2.5)	0.58 (−3 %)	−27.0 (−1.1)	1.8 (−0.7)
122 ka	−28.1 (+0.2)	−11.9 (+1.0)	0.62 (+3 %)	−25.1 (+0.8)	3.0 (+0.6)
126 ka	−27.4 (+0.9)	−7.1 (+5.8)	0.68 (+13 %)	−22.3 (+3.6)	5.2 (+2.7)

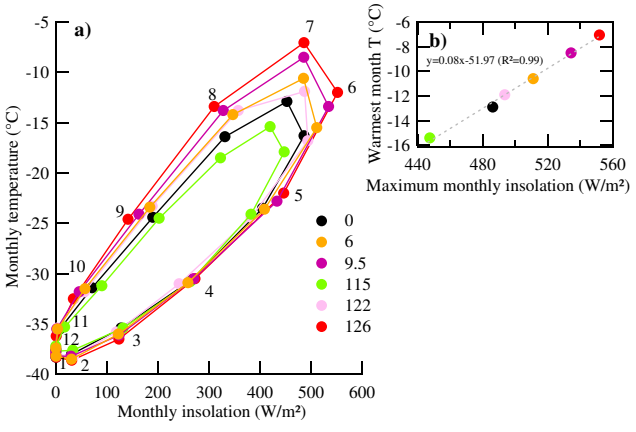

Fig. 2. **(a)** Seasonal cycle of IPSL model simulated central Greenland (>1300 m) temperature (°C) as a function of the seasonal cycle of TOA incoming solar radiation at 75° N (W m^{-2}) for different orbital configurations (0, 6, 9.5, 115, 122 and 126 ka). For each period, the monthly data are displayed; black numbers indicate the number of the month (from 1 for January to 12 for December). The elliptic shape results from the phase lag between temperature and insolation. **(b)** Regression between maximum monthly insolation and the IPSL model central Greenland maximum monthly summer temperature (occurring one month after maximum insolation). A linear relationship is observed, with a slope of 0.08 °C per W m^{-2}. The same color code is used as in panel a for the various simulations.

When taking into account the ocean circulation changes linked with a parameterization of Greenland melt at 126 ka, the IPSL-CM4 model simulates a 0.6 °C weaker July (resp. 0.4 °C annual) warming than in the standard 126 ka simulation (not shown in Table 2). In this simulation, the AMOC is weakened because deep water formation in the North Atlantic/Nordic Seas is reduced by the Greenland ice sheet meltwater. The meridional heat transport by the atmospheric circulation is enhanced to compensate for the reduction in ocean heat transport but the Arctic cools because of a larger sea ice extent. Therefore, taking into account the impact of ice sheet melting on the ocean circulation increases the model-data mismatch.

3.3 Differences between increased CO_2 and orbitally forced IPSL-CM4 climate responses

The orbital forcing has a negligible impact as such on the global and annual radiative forcing (<0.3 W m^{-2} over the last 130 ka), which contrasts with the 3.7 W m^{-2} radiative forcing for $2 \times CO_2$ (resp. 7.4 W m^{-2} for $4 \times CO_2$). Note that obliquity affects the latitudinal distribution of annual insolation, with opposite effects at low and high latitudes (not shown), and a range of variations of resp. 4.5 to 10.5 W m^{-2} at 75° N along the current and last interglacial (0–12 ka and 115–130 ka).

Moreover, the diurnal and seasonal distributions of orbital and $2 \times CO_2$ forcings are drastically different. For 126 ka, anomalies (relative to pre-industrial) in summer insolation exceed 50 W m^{-2} at mid and high northern latitudes (Fig. 3a, showing TOA radiative budget) at 126 ka, with large seasonal and latitudinal contrasts (Fig. 3b). This differs from the more homogeneous forcing caused by increased CO_2 concentrations.

We now focus on the 126 ka simulation, because of the large magnitude of the seasonal insolation change caused by the combination of precession and eccentricity for this period, and compare it with the $2 \times CO_2$ simulation. Figure 3 (panels c and d) shows the differences between last

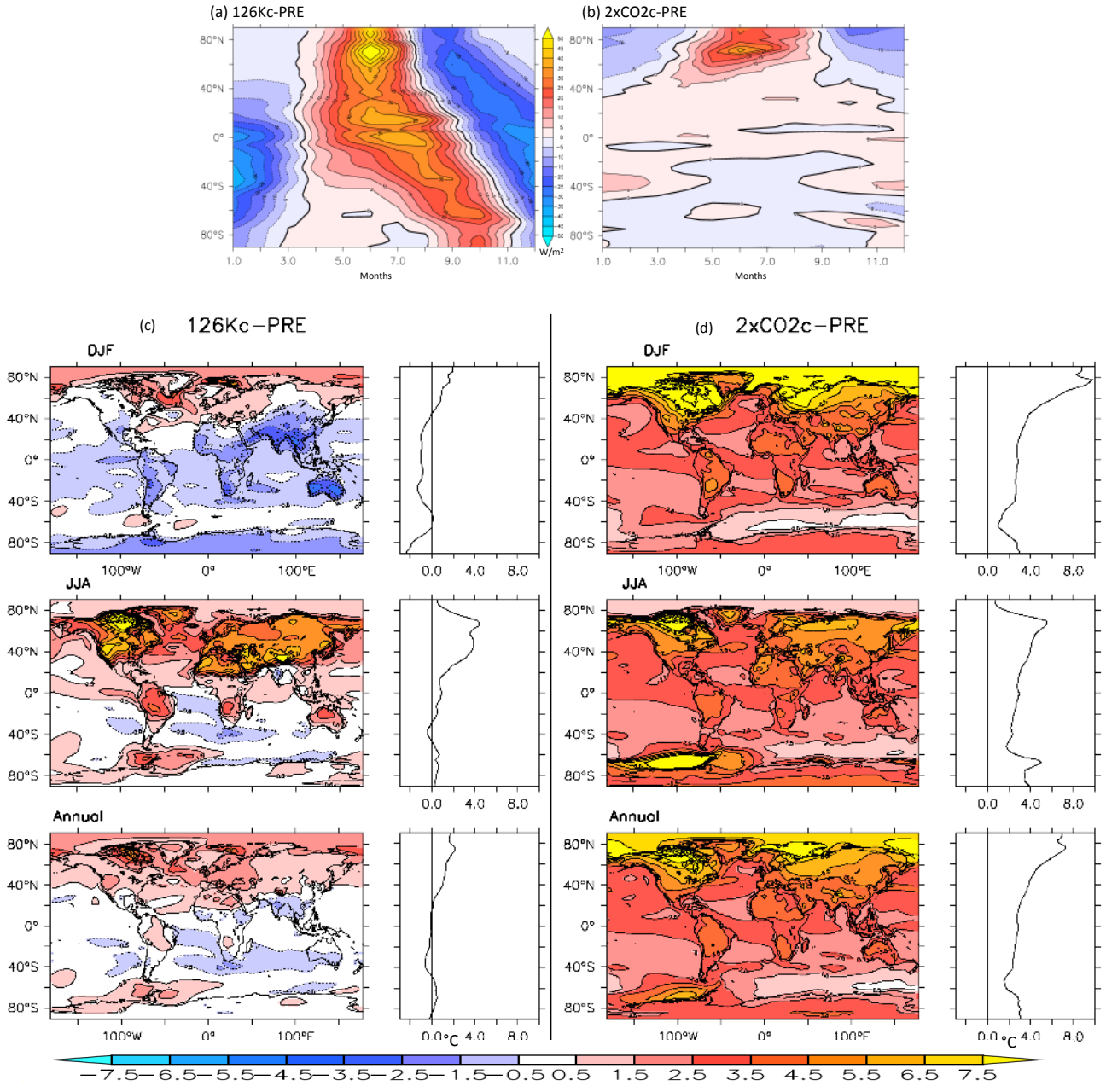

Fig. 3. Comparison of anomalies between the last interglacial and pre-industrial control IPSL model simulations (left panel) and $2 \times CO_2$ and pre-industrial control simulation (right panel) for : **(a)** and **(b)** TOA net radiative budget ($W\,m^{-2}$); **(c)** and **(d)** surface air temperature (°C) and **(e)** and **(f)** evaporation ($mm\,day^{-1}$). For panels **(a)** and **(b)**, anomalies are displayed as a function of month number (horizontal axis) and latitude (vertical axis). For panels **(c)** to **(f)**, anomalies are displayed as a function of longitude and latitude, for DJF (December-January-February), JJA (June-July-August) and for the annual mean. On the right side of each panel **(c)** to **(f)**, zonal mean anomalies are also displayed as a function of latitude.

interglacial (126 ka) and pre-industrial for JJA, DJF and annual mean temperature, as well as their zonal mean, and compares them to the differences between $2 \times CO_2$ and present day for JJA, DJF and annual mean temperature. Increased CO_2 leads to simulated warming at low latitudes and a larger magnitude of warming at both poles (relative to pre-industrial control simulation), especially in the winter season. By contrast the 126 ka orbital forcing leads to a small annual mean cooling at low to mid latitudes, a small annual mean warming anomaly around 60° S and a large (∼4 °C) warming in the Arctic. The model response to 126 ka orbital forcing follows the latitudinal and seasonal anomalies of

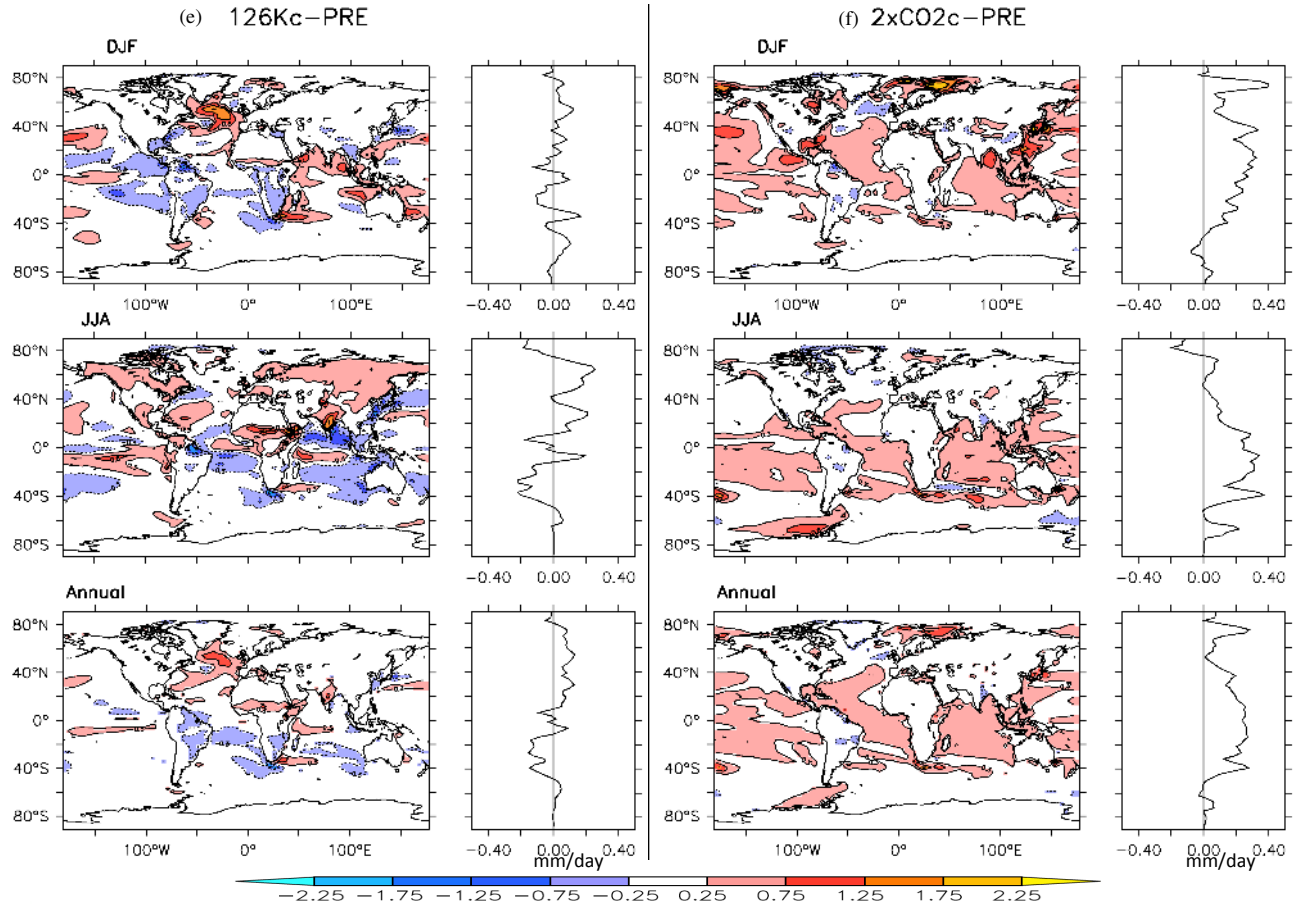

Fig. 3. Continued.

insolation (Fig. 3a), with the exception of the Arctic, where a year round persistent warming is simulated. Such a feature is model-dependent, as shown by the comparison between the IPSL-CM4 results and other coupled model simulations for the seasonal cycle of simulated last interglacial temperature anomalies for Greenland (Masson-Delmotte et al., 2010c).

Figure 4 shows that the control simulation correctly captures the amplitude and extrema of the observed Northern Hemisphere sea-ice cover (Rayner et al., 2003), but has a slight shift (one month earlier than in the data) in the seasonal cycle. In response to 126 ka orbital forcing, the model produces a summer sea ice retreat of ∼3 million km^2. This represents half of the retreat (∼6 million km^2) simulated for 2x × CO_2. In the 126 ka simulation, a small winter sea ice retreat is also simulated. This can be attributed to the large uptake of heat during summer in the high latitude ocean as well as to an enhanced AMOC, which brings warm surface waters to the high latitudes (Born et al., 2010). This winter sea-ice retreat is probably the cause for the warmer winter temperatures at 126 ka compared to the control simulation (Fig. 3c).

Winter Arctic warming is particularly large under 2 × CO_2 forcing, reaching ∼8 °C, compared to the ∼2 °C Arctic warming for 126 ka conditions. While this comparison highlights the differences between the two types of simulations, and therefore the limitations of analogies between the last interglacial and future climate change, we would like to stress that the simulated summer Arctic warming at 126 ka reaches a magnitude (∼4 °C) comparable to summer Arctic warming forced by 2 × CO_2 (see also Fig. 5d).

The different climate responses to orbital (126 ka) and 2 × CO_2 forcing are also shown on the global pattern of evaporation changes. Figure 3e shows a strong increase in summer North Atlantic evaporation at 126 ka, in contrast with a strong increase in Nordic Seas evaporation in response to 2 × CO_2 forcing (probably linked with reduced sea-ice cover). We hypothesize that changes in moisture sources affect moisture distillation and Greenland precipitation isotopic depletion, and therefore the isotope-temperature relationships. Before presenting the isotopic calculation results (in Sect. 4), we perform a simple analysis of radiative feedbacks in order to understand the causes of the linear behavior of the IPSL-CM4 model in response to orbital forcing, and to further compare the model response to CO_2 and orbital forcing.

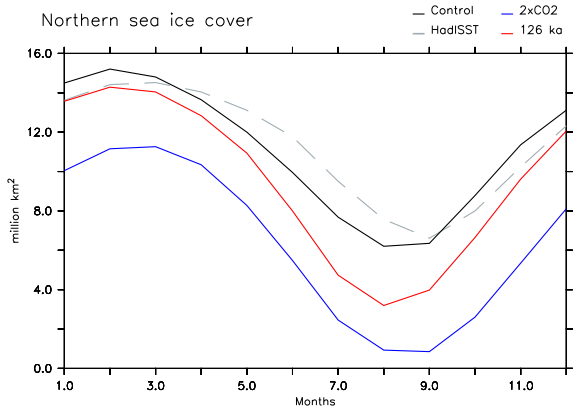

Fig. 4. Monthly seasonal cycle of Northern Hemisphere sea ice extent for present day (black), 126 ka (red) and $2 \times CO_2$ (blue) simulated by IPSL-CM4. Present day (1900–2010) climatological data (Rayner et al., 2003) are also displayed (dashed grey).

3.4 Analysis of radiative feedbacks

Following Braconnot et al. (2007), a simple feedback analysis was performed in order to quantify the main drivers of changes in the top of the atmosphere radiative budget (TOA) at high latitudes (60–80° N). The methodology for this analysis is described in Appendix A.

Figure 5 displays analyses of the TOA radiative budget terms and key feedbacks (represented by symbols) around Greenland. The different simulations are represented by the same colors as in Fig. 2. The specific radiative budgets for June–July are shown for all the orbitally forced simulations (Fig. 5a) and for each month for 126 ka (Fig. 5b) and $2 \times CO_2$ simulations (Fig. 5c). We do not display the changes in heat and water transport and only focus on the local radiation fluxes within the atmospheric column.

Figure 5a characterises the radiative feedbacks involved in the linear response of the IPSL-CM4 simulated summer Greenland surface temperature with respect to summer insolation. At high northern latitudes, the different components of the radiative budget depict a linear relationship with respect to the change in incoming solar radiation at the top of the atmosphere ΔSWi_{simul}. The net TOA shortwave flux (ΔSWn_{simul}, represented by "x"symbols) appears relatively close to the prescribed insolation change and only partially compensated for by increased longwave emission (ΔLWn_{simul}, represented by filled diamonds) so that the net radiative budget is positive (not shown).

At 6, 9.5, 122 and 126 ka, a strong positive shortwave feedback is linked with the total (surface and cloud) albedo effect (ΔALB_{simul}, represented by "+" symbols). This effect is dominated by the clear sky (surface) albedo effect ($\Delta ALB\,cs_{simul}$ represented by the triangle symbols), only partly compensated by an enhanced negative cloud shortwave feedback (difference between $\Delta ALB\,cs_{simul}$ and ΔALB_{simul}). The albedo feedback is consistent with changes in sea ice (Fig. 4). It increases almost linearly with the insolation forcing, stressing that the changes in clear sky shortwave surface radiation drive the surface radiative budget, surface temperature and thereby the snow and ice extent. Note that by construction, the total albedo feedback between the different simulations lies on a line proportional to the planetary albedo of the control simulation. At 115 ka, clear sky and cloud albedo feedbacks have opposite signs and have a much smaller magnitude (with respect to the magnitude of the orbital forcing) compared to other orbital simulations. The different effects are thus not symmetrical for increased or reduced insolation, certainly due to the temperature thresholds needed to build and melt snow and ice.

In addition, the longwave radiative budget changes (ΔLWn_{simul}, filled diamonds) appear to be driven by the changes in Planck emission directly caused by changes in surface temperature (ΔPl_{simul}, open diamonds). There is only a small increase in the atmospheric greenhouse effect caused by changes in the vertical temperature profile, water vapour content, and infra-red cloud radiative feedbacks (difference between the filled and open diamond symbols). This greenhouse feedback is too small to drive a non-linear response of the radiative budget around Greenland.

While this approach ignores the dynamical heat advection effects, it suggests that the top of the atmosphere radiative budget at high northern latitude is relatively linear with respect to orbital forcing and highlights the importance of the positive feedbacks linked with the surface albedo. The magnitude of the atmospheric greenhouse effect and the shortwave cloud negative feedback increase with the magnitude of the insolation forcing. In this model, the cloud feedback is enhanced for a warmer Arctic. Compensations of non-linearities of the Planck, albedo and cloud radiative effects at 115 ka likely explain the overall linearity of the IPSL-CM4 model high northern latitude temperature response to summer insolation forcing.

Figure 5b and c show a comparison of the seasonal cycle and magnitude feedbacks at play in 126 ka and $2 \times CO_2$ simulations, respectively. As previously mentioned, they reach similar magnitudes of summer temperature change over Greenland. As expected, the changes in greenhouse effect are larger for the $2x \times CO_2$forcing than for insolation forcing. The net radiative budget is positive in summer. The net shortwave radiation reflects the total albedo effect. Again, the clear sky albedo feedback is the dominant contribution during summer, and the cloud feedback only accounts for a small fraction of changes in shortwave radiation, even though its magnitude is larger than for the insolation forcing. This comparison shows that the albedo, cloud and atmospheric greenhouse feedbacks have comparable magnitude and sign in summer. These simulated feedbacks seem consistent with ongoing changes related with Arctic sea-ice retreat and warming (Screen and Simmonds, 2010). This analysis also highlights the different seasonality effects, with

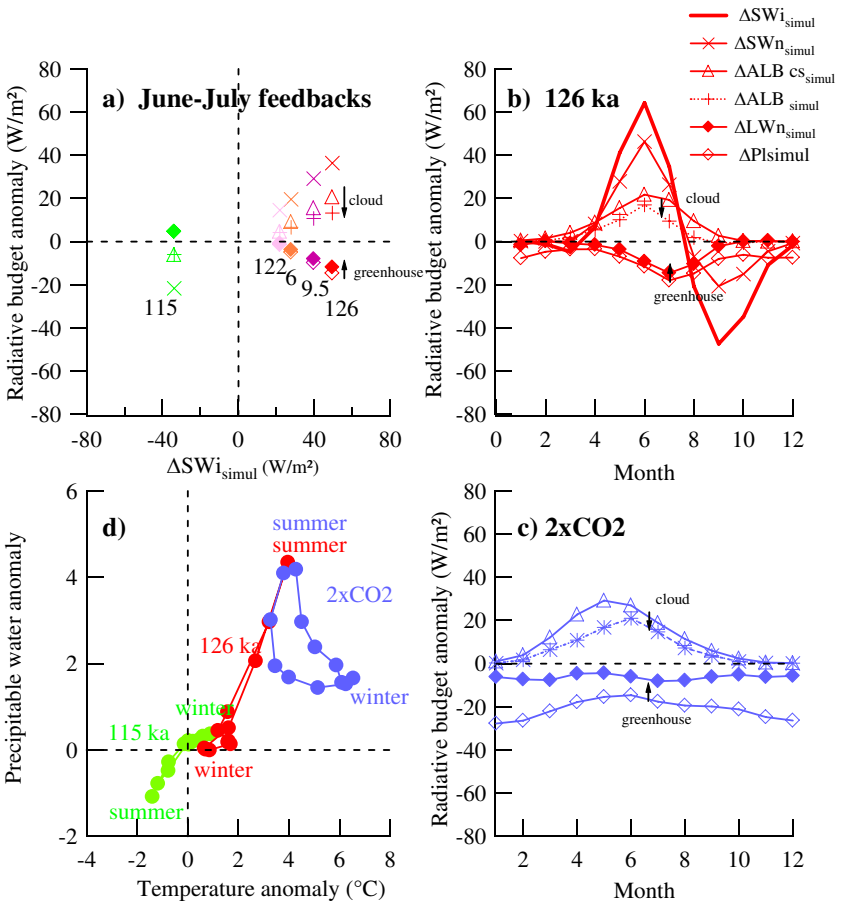

Fig. 5. Analysis of atmospheric feedbacks affecting the TOA radiative budget. **(a)** June–July changes in radiative budget terms (see text and figure legend for details) as a function of June-July incoming solar radiation ($W\,m^{-2}$), for different orbital contexts (6 ka, orange; 9.5 ka, violet; 115 ka, green; 122 ka, pink; and 126 ka, red). Arrows depict the magnitude of albedo (difference between "+" and triangle symbols), cloud (difference between "+" and "x" symbols) and greenhouse (difference between open and filled diamonds) feedbacks for 126 ka. **(b)** Monthly values of the radiative budget 126 ka anomalies with respect to the control simulation (see text and legend for details) ($W\,m^{-2}$). **(c)** Same as **(b)** but for $2 \times CO_2$. **(d)** Seasonal cycle of precipitable water anomaly as a function of temperature anomaly (°C) with respect to the control simulation, for 115 ka (green), 126 ka (red) and $2 \times CO_2$ (blue).

larger greenhouse feedbacks for $2 \times CO_2$ in winter, as well as an earlier albedo feedback for $2 \times CO_2$, likely caused by the strongly reduced winter sea-ice cover in this simulation than for 126 ka (Fig. 4).

In order to better characterize the links between changes in surface temperature and atmospheric water content, Fig. 5d compares the seasonal cycle of atmospheric precipitable water anomaly as a function of surface temperature anomaly for 115, 126 ka and $2 \times CO_2$ simulations. The asymmetry between atmospheric moisture changes at 115 and 126 ka is obvious. Despite a completely different seasonality of the changes (with the $2 \times CO_2$ simulations showing its largest temperature changes in winter), the 126 ka and $2 \times CO_2$ simulations again depict similar magnitudes of temperature and precipitable water changes, in summer.

4 Atmospheric modeling of water stable isotopes

4.1 Set up of the LMDZiso simulations

While water stable isotopes are not yet available in the coupled IPSL-CM4 model, they have been implemented in its atmospheric component, LMDZ4 (Risi et al., 2010b) (hereafter called LMDZiso), with a standard resolution of 2.5° × 3.75°. The ability of the model to capture the modern and Last Glacial Maximum (LGM) Greenland precipitation isotopic composition has been previously analysed (Risi et al., 2010b; Steen-Larsen et al., 2011). These comparisons have shown that the model correctly captures the 0.8 ‰ per °C modern spatial isotope-temperature relationship obtained from Greenland data (see Sect. 2). In central and North Greenland, the model has a warm bias (up to 8 °C) and produces too enriched precipitation (by 5 ‰). This contrasts with a cold

and enriched bias at coastal stations. Comparable biases are found by other atmospheric models that include water stable isotopes (e.g. ECHAM and REMO-iso) (Sjolte et al., 2011).

A suite of simulations has been conducted with the LMDZiso model, forced by the sea surface conditions and associated external forcings (6 ka and 126 ka orbital parameters, and increased greenhouse gas concentrations) simulated by the IPSL-CM4 model; a sensitivity test with 4 °C homogeneous artificial increase in sea surface temperature compared to present-day (AMIP) has also been performed (Table 1). The isotopic simulations were run for 5 years, which is sufficient for the equilibration between the atmosphere and land surface reservoirs. We verified that trends in temperature and stable isotopes over Greenland over the first 3 years of the simulations are lower than the standard deviations of the last 3 years, which were used for this study. We also verified, using a longer 126 ka simulation (16 years), that the standard deviations calculated over a period of 3 years were not decreasing with a longer spin up period.

4.2 LMDZiso isotope-temperature relationships

Consistent with the coupled IPSL-CM4 simulations discussed in Sect. 3, annual mean temperature changes simulated in central Greenland remain very small for the simulations corresponding to changes in orbital configurations (<1 °C) (Fig. 6). They reach 4 °C for $2 \times CO_2$, 6 °C for SST + 4 °C and ∼9 °C for $4 \times CO_2$ simulations (Fig. 7). Deposition effects can be considered both for temperature and $\delta^{18}O$ by calculating either annual mean or precipitation weighted values (Fig. 7). As discussed previously, this effect is particularly large for the orbitally forced simulations (up to 2 °C and 1 ‰, reaching magnitudes comparable to the climate change signal). Because the CO_2 forcing increases both winter and summer temperature and precipitation (Fig. 6), the resulting precipitation weighting effect is smaller (typically 1 °C and 0.5 ‰ for $4 \times CO_2$). This effect enhances the magnitude of precipitation weighted $\delta^{18}O$ anomalies (Fig. 7) and therefore slightly increases the "warm climate" isotope-temperature slope (from 0.30 to 0.36 ‰ per °C). Within all the studied simulations, the strength of the correlation is comparable between annual mean precipitation isotopic composition and temperature, and precipitation weighted isotopic composition and temperature ($R^2 > 0.95$, $n = 6$) and larger than the correlation between precipitation weighted isotopic signal and annual mean temperature ($R^2 = 0.86$, $n = 6$). This suggests that the ice core data (capturing precipitation weighted information) should best be interpreted in terms of changes in precipitation-weighted temperature.

When considering all the available simulations, a linear regression leads to a mean "warm climate" isotope-temperature slope of 0.31 ‰ per °C, with values ranging from 0.26 to 0.39 ‰ per °C. This uncertainty is estimated by using either annual mean or precipitation weighting for

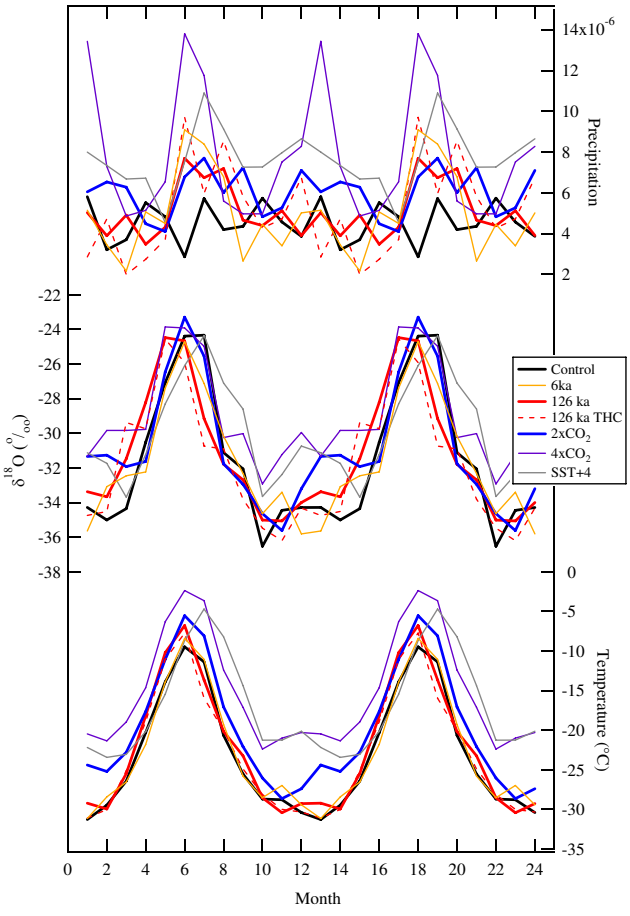

Fig. 6. Monthly seasonal cycle of temperature, precipitation and precipitation $\delta^{18}O$ simulated by LMDZiso for different sets of boundary conditions (AMIP control, 6 ka, 126 ka, +4 °C SST, 2 × and 4x × CO_2 concentrations) prescribed using the IPSL-CM4 sea surface conditions (see Table 1). For readability, the seasonal cycle has been repeated over 2 years (24 months).

temperature and $\delta^{18}O$, and by selections of 5 of the 6 simulations to assess the uncertainty on each slope, which is about 0.03 ‰ per °C. This simulated slope is consistent with the lowest values derived from interstadial warming events (Capron et al., 2010a), with the slopes obtained using the borehole information at the glacial-interglacial scale (Cuffey and Clow, 1997; Dahl-Jensen et al., 1998), and lower than the slopes estimated during the current interglacial period after accounting for elevation changes (Vinther et al., 2009). This finding is also consistent with a small isotope-temperature slope simulated by the GISS model for the Holocene for Greenland (Legrande and Schmidt, 2009).

At 126 ka, the simulated change in Greenland precipitation isotopic composition is very small (0.75 ‰) compared to the ice core data. Indeed, a ∼3 ‰ anomaly above the last millennium level is consistently recorded in the deepest part of the NorthGRIP ice core (at 123 ka), in ice from the last interglacial found in the disturbed bottom layers

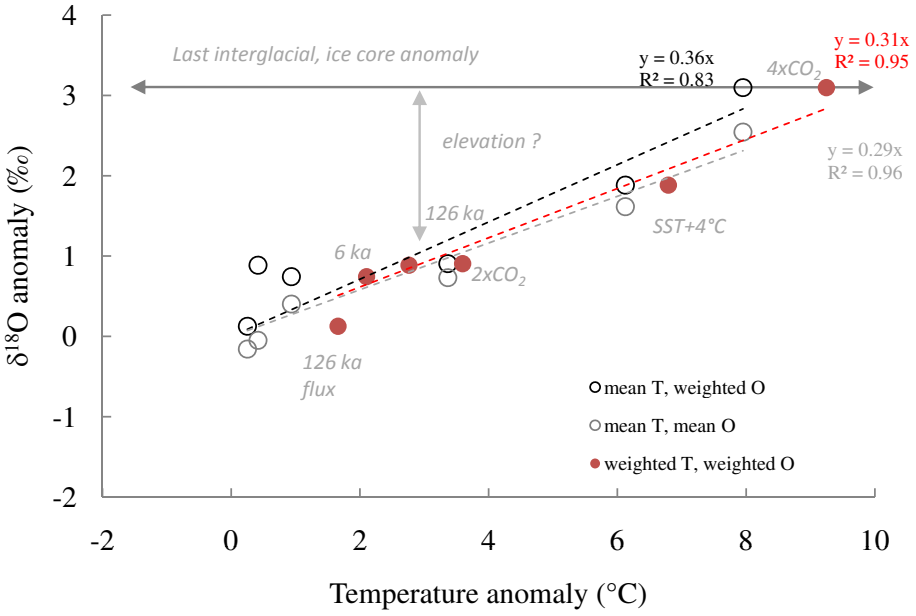

Fig. 7. Simulated anomalies of Greenland precipitation-weighted δ^{18}O as a function of mean temperature (black open circles) and precipitation-weighted temperature (red filled circles). Simulated anomalies of Greenland annual mean δ^{18}O as a function of annual mean temperature (grey open circles) are also displayed for all the LMDZiso simulations. Anomalies are calculated with respect to the AMIP control simulation. Linear regressions are also displayed.

at Summit (Landais et al., 2004; Masson-Delmotte et al., 2010a; Suwa et al., 2006) and in preliminary measurements from the NEEM ice core, recently drilled in northwestern Greenland (unpublished data).

The deposition effect alone cannot explain why the isotope-temperature slope is particularly weak for these warmer-than-present climates. Larger spring-summer temperature anomalies in the $4 \times CO_2$ simulation are only associated with a small Greenland precipitation δ^{18}O anomaly. This is also the case, but in a weaker proportion, for the 126 ka simulation. Source effects linked with geographical shifts of the origin of the moisture source (as hinted by changes in evaporation, Fig. 3) are likely the cause for a reduced isotopic depletion despite strong summer Arctic warming.

4.3 LMDZiso changes in moisture origin

We conducted a water tagging experiment (Risi et al., 2010a) in which the high latitude (North of 50° N) oceanic evaporation was tagged for the control and $4 \times CO_2$ experiments (in order to explore the largest anomaly). For central Greenland, 14 % of present-day moisture originates from high latitude (>50° N) evaporation. High latitude evaporation is strongly isotopically enriched compared to the global mean atmospheric water vapour. The modern spatial slope in Greenland is 0.8 ‰ per °C including all moisture sources. The water tagging simulation shows that, without the Arctic moisture source, this spatial slope would be reduced to 0.7 ‰ per °C. This arises from a spatial gradient in the contribution of (enriched) high latitude moisture to Greenland precipitation. This contribution decreases poleward, because air mass trajectories reaching northern Greenland are transported at high elevation and are less exposed to high latitude evaporation.

In the $4 \times CO_2$ experiment, the proportion of high latitude moisture decreases by about 40 % in winter and 60 % in summer, due to enhanced poleward moisture transport from the subtropics and decreased high latitude evaporation (Fig. 3). This source effect quantitatively explains the difference between the Rayleigh isotope-temperature slope (0.7 ‰ per °C) and the actual temporal isotope-temperature slope (0.3 ‰ per °C). This analysis shows that changes in high latitude recycling explain why the isotope-temperature slopes for warmer climates are much smaller in LMDZiso than the modern spatial slope. We now compare the LMDZiso model results with other available isotopic model results.

4.4 Comparison with other isotope model results

Small slopes are simulated by the LMDZiso model for Greenland for projections and interglacial configurations, and by the GISS model for the Holocene for Greenland (Legrande and Schmidt, 2009).

Here we also briefly examine results from Greenland using HadAM3iso simulations previously published for Antarctica (Sime et al., 2008). We focus on a snapshot simulation for the year 2100 in response to SST and sea ice outputs from the coupled Hadley model simulation using the A1B greenhouse

concentration scenario. This is relatively comparable to the LMDZiso $2 \times CO_2$ simulation.

Whilst seasonal cycles of LMDZiso $2 \times CO_2$ and HadAM3iso 2100 outputs show relatively comparable magnitudes of Arctic sea ice, central Greenland temperature and precipitation changes, albeit with slightly different seasonal aspects (Supplement, Fig. S1), $\delta^{18}O$ anomalies (with respect to the reference period) are higher for HadAM3iso (not shown). The HadAM3iso $\delta^{18}O$ anomalies are positive all year round, while LMDZiso $2 \times CO_2$ shows very small (or slightly negative) $\delta^{18}O$ anomalies for that season. As a result, the HadAM3iso model produces larger shifts in $\delta^{18}O$ for a comparable warming, compared with LMDZiso. The average central Greenland shift is about 3 ‰ in HadAM3iso, which is slightly closer to the observed interglacial shift, compared with LMDZiso. However, note that since this shift occurs due to CO_2 forcing, rather than a more realistic orbital forced warming, it is difficult to know the pertinence of this result for the last interglacial climate.

The difference between the models likely arises from differences in moisture advection to central Greenland. HadAM3iso 2100 evaporation changes have comparable patterns but larger magnitudes at high northern latitudes, compared to $2 \times CO_2$ LMD4iso results (Figs. 3 and 8). This suggests that, whilst LMDZ4iso enhances the transport of depleted subtropical moisture towards Greenland (see previous section), the specific 2100 simulation examined here may be allowing HadAM3iso to transport more moisture from nearby sea ice free high latitude oceans during the CO_2 warming. Present day observations also depict shifts between local and advected moisture during the autumn ice growth season with distinct isotopic fingerprints which also tends to support the idea that this local-distal moisture transport balance mechanism could be important (Kurita, 2011).

We conclude from this that changes in deposition (bias towards summer precipitation for orbitally driven warm climates) and source effects (varying contribution of Arctic moisture for all simulations) are responsible for the LMDZiso Greenland isotope-temperature slope being smaller than the modern spatial slope for warmer-than-present climates. The magnitude of changes in moisture origins and transport pathways could affect the isotope-temperature slope between different models and different simulations. Additional investigations (differences in surface boundary conditions, isotopic composition of the atmospheric water vapor, moisture advection paths) are needed to assess better and understand the reasons for inter-model differences.

4.5 Implications of IPSL-CM4/LMDZiso results for central Greenland ice sheet elevation during the last interglacial

The LMDZiso low temporal slope appears consistent with previous results obtained for glacial (Capron et al., 2010a) and Holocene (Vinther et al., 2009) climates. The IPSL-CM4 and LMDZiso models do underestimate the magnitude of temperature and precipitation isotopic composition changes compared to the ice core data. This mismatch may result from either missing feedbacks (e.g. vegetation changes), model sensitivity to forcings (e.g. magnitude of sea ice, water vapour and moisture origin, cloud etc. feedbacks), or, alternatively, from changes in Greenland elevation, which are not considered in the climate simulations.

Assuming that the LMDZ/IPSL-CM4 model correctly captures the first order of the response to 126 ka insolation, the model-data comparison leaves a $\delta^{18}O$ anomaly of $\sim$2.25 ‰ to explain. Given the modern ~ -0.6 ‰ per 100 m $\delta^{18}O$-elevation gradient in Greenland (Vinther et al., 2009), this suggests that the central Greenland ice sheet elevation may have been reduced by at most 325–450 m at the end of the last interglacial. Such a reduced elevation in central Greenland is expected to result from stronger melt in the coastal ablation zone and dynamical ice sheet response during the last interglacial compared to today. So far, no information can be extracted from the deepest parts of the NorthGRIP ice core regarding elevation changes. Air content measurements from the deepest parts of the GRIP ice core (Raynaud et al., 1997) suggest little change in Summit elevation. It is expected that the undisturbed parts of the NEEM ice core could bring further constraints.

Simulations including the parameterization of Greenland melt at 126 ka produce, however, a reduced AMOC and limited Greenland warming (reduced by 0.6 °C in summer and 0.4 °C in annual mean compared to the standard 126 ka simulation), further reducing the magnitude of the simulated change in annual temperature and precipitation isotopic composition. In this case (not shown), LMDZiso produces a very small precipitation weighted $\delta^{18}O$ anomaly (0.13 ‰) (Fig. 7) which increases the model-data mismatch and would require larger elevation changes (400 to 1000 m, depending on the isotope-elevation slope) to bring the climate simulations in agreement with the NorthGRIP data. This result calls for consistent analyses of the estimates of the ice-sheet feedbacks at the regional scale in central Greenland (elevation effects) and at the larger scale (impacts on the thermohaline circulation and consequences for Arctic-Greenland climate, water cycle and stable isotopes).

5 Conclusions and perspectives

This manuscript has explored several aspects of past interglacials in Greenland from the available ice core information and the perspective of climate-isotope modeling.

The ice core data, within age scale uncertainty, show a lagged response of $\delta^{18}O$ optima with respect to precession within a few millennia. It is very likely that these optima are caused by ice sheet response to insolation, modulating the Greenland surface elevation (affecting the ice core

temperature records) and the large-scale ocean circulation and climate (through the meltwater flux). Parallel decreasing trends between Northern Hemisphere summer insolation and ice core stable isotope data are found at the end of the current and last interglacials, albeit with different magnitudes of slopes. New information is expected from the NEEM deep ice core. There is data-based evidence from other paleothermometry methods (borehole data for the Holocene to last glacial variability, gas thermometry during abrupt glacial warming events) that the isotope-temperature slope varies between 0.3 and 0.6 ‰ per °C.

The comparison between climate model simulations and ice core data is obviously complicated by uncertainties on the ice sheet topography and the impact of ice sheet melting on ocean circulation (as forcings for coupled ocean-atmosphere models), and also by the uncertainties on the isotope-temperature slopes. Here, we make use of coupled ocean-atmosphere simulations, using IPSL-CM4, under different orbital and CO_2 forcings.

At 126 ka, this model has a strong summer temperature response compared to earlier published runs (e.g. .Otto-Bliesner et al., 2006; Gröger et al., 2007), and propagates the orbitally forced summer Arctic warming towards winter season. There is evidence for a strong sea ice retreat in some Arctic areas during the last interglacial (Polyak et al., 2010), possibly larger than in the IPSL-CM4 simulations. New sea ice proxy records would be extremely useful to assess the realism of the modeled sea ice response. In these simulations, the IPSL-CM4 model does not include the feedbacks associated with vegetation changes. Increased boreal forest cover (CAPE, 2006) could be expected to induce continental spring warming due to the albedo effect, and summer cooling due to increased evapotranspiration (Otto, 2011).

The IPSL-CM4 model depicts a very strong linear relationship between simulated summer Greenland temperature and summer insolation forcing from 6 orbital configurations (0, 6, 9.5, 115, 122 and 126 ka). The slope of this relationship appears smaller than the one which can be estimated from the NorthGRIP data for the late interglacial trends. This may be due to the lack of feedbacks such as ice sheet elevation changes. Sensitivity tests with parameterisations of Greenland melt however highlight the fact that a large Greenland meltwater flux (about 10 mm yr^{-1}) (Swingedouw et al., 2009) acts as a local negative feedback through the impact of a reduced AMOC, decreasing the magnitude of 126 ka Greenland warming by about 0.5 °C. These tests, however, do not account for any changes in Greenland ice sheet topography.

The quantitative interpretation of the ice core data relies on estimates of the temporal isotope-temperature relationship. Because the simulated 126 ka annual mean temperature change is modest (<1 °C), and lower than expected from the ice core data, we also explore simulations conducted using boundary conditions from $2 \times CO_2$ and $4 \times CO_2$ as well as 4 °C warmer SST climates. Because there is no physical analogy between the greenhouse and orbital forcings, the IPSL-CM4 model response strongly differs in terms of seasonal and latitudinal temperature or water cycle changes. Inter-model differences in their response to orbital and greenhouse forcing can however be large.

During the last interglacial, the mid to high latitude summer warming occurs without a clear tropical or global anomaly and persists in winter at high latitudes; obliquity changes indeed induce reduced annual mean tropical insolation and ocean temperatures. This strongly differs from the impact of increased greenhouse gas concentrations, marked by year round tropical warming and strong winter warming at high latitudes. However, the magnitude of summer Arctic warming is very similar in the IPSL-CM4 126 ka and $2 \times CO_2$ simulations. Moreover, our simple analysis of feedbacks affecting the TOA radiative budget has also demonstrated comparable magnitudes of changes in the albedo, cloud and atmospheric greenhouse feedbacks in summer. Given the importance of summer temperature on ice sheet ablation, these comparable magnitudes have relevance regarding the assessment of climate model feedbacks, changes in Greenland ice sheet mass balance, and implications for sea level.

The LMDZiso model outputs show strong shifts in the precipitation seasonality due to increased summer precipitation in response to the 6 ka and 126 ka orbital forcings (proportionally stronger than for increased CO_2 simulations). If true, this suggests that the Greenland ice core interglacial data must be cautiously interpreted in terms of precipitation weighted signals with a summer bias. In the warm climate simulations, LMDZiso produces an isotope-temperature slope of ∼0.3 ‰ (within a 30 % uncertainty). Shifts in moisture origin under warm summer conditions clearly reduce the imprint of Greenland temperature changes in the simulated $\delta^{18}O$. Such changes may be caused by changes in storm tracks or in the Hadley cell (Fischer and Jungclaus, 2010), in response to changing latitudinal temperature gradients, sea ice and land sea contrasts. The differences between isotopic model $\delta^{18}O$ shifts may be due to different changes in moisture origin (especially the proportion of Arctic versus low latitude moisture). This aspect would deserve to be further investigated, perhaps using water tagging methods, and/or second order stable isotope information (e.g. deuterium excess, oxygen 17-excess) which could allow the realism of changes in moisture source characteristics to be tested (Kurita, 2011).

For LMDZiso, the simulated 6 ka and 126 ka $\delta^{18}O$ is much weaker than the ice core signals. Given the range of isotope-temperature responses obtained under strongly warmer climates (+4 °C SST, $4 \times CO_2$), the last interglacial ice core signal (∼3 ‰) is only compatible with very large (precipitation-weighted) temperature shifts (8 to 10 °C) (at fixed elevation). The 126 ka LMDZiso simulation can also be reconciled with the ice core data, assuming a 300–400 m reduced elevation in central Greenland (and even larger surface elevation changes

when considering the impact of meltwater on climate). In the future, this should be compared with information obtained from air content data (Raynaud et al., 1997) from the recent NEEM deep ice core, and with ice sheet model results (Otto-Bliesner et al., 2006; Robinson et al., 2011). The robustness of this finding should be assessed by comparing last interglacial precipitation isotopic composition simulations conducted with different climate models.

In the coming years, the PMIP3 project is expected to allow climate model inter-comparison with standardized boundary conditions for the last interglacial. We also aim to perform simulations at 126 ka with a prescribed reduced Greenland ice sheet, in order to better assess the impact of elevation changes on temperature and precipitation isotopic composition. Intercomparisons of isotopic simulations both under last interglacial and increased CO_2 boundary conditions are needed in order to better understand the robustness of the results. Such analysis could be also expanded to Antarctica, where the cause for the ice core $\delta^{18}O$ optimum remains debated but is of considerable interest (Holden et al., 2010; Laepple et al., 2011; Masson-Delmotte et al., 2010c; Sime et al., 2009). Finally, the consistency between interglacial changes in elevation, accumulation and meltwater fluxes would benefit from robust assessment. A good framework for this lies in coupling a water stable isotope tracer enabled interactive ice sheet- climate with a fully isotopically enabled climate model.

Appendix A

Method for radiative feedbacks analysis

Following (Braconnot et al., 2007), a simple feedback analysis was performed in order to quantify the main drivers of changes in the top of the atmosphere radiative budget (TOA) over and around Greenland (60–80° N, 60–10° W):

$$\Delta \mathrm{TOA}_{\mathrm{simul}} = \Delta \mathrm{SWn}_{\mathrm{simul}} + \Delta \mathrm{LWn}_{\mathrm{simul}} \quad \text{(A1)}$$

where Δ_{simul} is the change between a forced simulation (6, 9.5, 115, 122, 126 ka and $2 \times CO_2$) and the control simulation (ctrl); SWn is the net shortwave radiation at the top of the atmosphere (positive downwards) and LWn the net longwave radiation (positive downwards).

$\Delta \mathrm{SWn}_{\mathrm{simul}}$ is driven by interplay between the insolation forcing and the albedo feedbacks. The actual insolation forcing $\Delta \mathrm{SWf}_{\mathrm{simul}}$ corresponds to the net change in shortwave radiative forcing under the assumption of a constant planetary albedo (Hewitt and Mitchell, 1996). The shortwave radiative forcing (SWf) (at fixed planetary albedo) is estimated using the control simulation planetary albedo ($\alpha^{\mathrm{tot}}_{\mathrm{ctrl}}$) and the prescribed change in insolation $\Delta \mathrm{SWi}_{\mathrm{simul}}$ as:

$$\Delta \mathrm{SWf}_{\mathrm{simul}} = \left(1 - \alpha^{\mathrm{tot}}_{\mathrm{ctrl}}\right) \ \Delta \mathrm{SWi}_{\mathrm{simul}}. \quad \text{(A2)}$$

The albedo feedback then results from the changes in surface albedo, atmospheric diffusion and clouds:

$$\Delta \mathrm{ALB}_{\mathrm{imul}} = \Delta \mathrm{SWn}_{\mathrm{simul}} - \Delta \mathrm{SWf}_{\mathrm{simul}}. \quad \text{(A3)}$$

At first approximation, for clear sky conditions (cs), the change in shortwave radiation at the top of the atmosphere is primary due to changes in surface albedo (even though one cannot distinguish the effects of changes in atmospheric properties from changes in surface albedo). The snow and sea ice albedo effect can be thus be approximated from the difference in simulated clear sky (cs) net shortwave radiative fluxes, as:

$$\Delta \mathrm{ALB\ cs}_{\mathrm{simul}} = \Delta \mathrm{SWn\ cs}_{\mathrm{simul}} - \Delta \mathrm{SWf}_{\mathrm{simul}}. \quad \text{(A4)}$$

The role of clouds on $\Delta \mathrm{SWn}_{\mathrm{simul}}$ can then be estimated as the difference between the total and clear sky albedo feedbacks, or equivalently, by the change in cloud shortwave radiative forcing (with small uncertainties resulting from the differences in the area covered by clouds in the different simulations).

It is not easy to estimate the contribution of surface temperature, water vapour content, trace gases and lapse rate on the long wave emission at the top of the atmosphere ($\Delta \mathrm{LWn}_{\mathrm{simul}}$). In the case of orbital forcing, all the terms that affect the longwave radiation are considered as feedbacks, which contrast with the $2 \times CO_2$ forcing that exerts a direct longwave forcing. Here, we only consider a bulk estimate of the total greenhouse effect (g), considering the difference between the long wave emission at the surface and at the top of the atmosphere

$$\Delta g_{\mathrm{simul}} = \Delta \mathrm{LWn}_{\mathrm{simul}} - \Delta \mathrm{Pl}_{\mathrm{simul}} \quad \text{(A5)}$$

with $\Delta \mathrm{Pl}_{\mathrm{simul}}$ the change in direct (Planck) emission at the surface temperature $\mathrm{Ts}_{\mathrm{simul}}$ with respect to the control simulation, which can be approximated by:

$$\Delta \mathrm{Pl}_{\mathrm{simul}} = 4\,\sigma\ \mathrm{Ts}^3_{\mathrm{ctrl}}\ (\mathrm{Ts}_{\mathrm{simul}} - \mathrm{Ts}_{\mathrm{ctrl}}). \quad \text{(A6)}$$

Supplementary material related to this article is available online at: http://www.clim-past.net/7/1041/2011/cp-7-1041-2011-supplement.pdf.

Acknowledgements. The research leading to these results has received funding from the French Agence Nationale de la Recherche (NEEM project) and from the European Union's Seventh Framework programme (FP7/2007-2013) under grant agreement n^o 243908, "Past4Future. Climate change - Learning from the past climate". This is PAST4FUTURE publication 10.

Edited by: M. Siddall

The publication of this article is financed by CNRS-INSU.

References

Alkama, R., Kageyama, M., Ramstein, G., Marti, O., Ribstein, P., and Swingedouw, D.: Impact of a realistic river routing in coupled ocean-atmosphere simulations of the Last Glacial Maximum climate, Clim. Dynam., 30, 855–869, 2008.

Barnola, J. M., Raynaud, D., Korotkevich, Y. S., and Lorius, C.: Vostok ice core provides 160,000-year record of atmospheric CO_2, Nature, 329, 408–414, 1987.

Born, A., Nisancioglu, K. H., and Braconnot, P.: Sea ice induced changes in ocean circulation during the Eemian, Clim. Dynam., 35(7–8), 1361–1371, 2010.

Braconnot, P., Otto-Bliesner, B., Harrison, S., Joussaume, S., Peterchmitt, J.-Y., Abe-Ouchi, A., Crucifix, M., Driesschaert, E., Fichefet, Th., Hewitt, C. D., Kageyama, M., Kitoh, A., Loutre, M.-F., Marti, O., Merkel, U., Ramstein, G., Valdes, P., Weber, L., Yu, Y., and Zhao, Y.: Results of PMIP2 coupled simulations of the Mid-Holocene and Last Glacial Maximum - Part 2: feedbacks with emphasis on the location of the ITCZ and mid- and high latitudes heat budget, Clim. Past, 3, 279–296, doi:10.5194/cp-3-279-2007, 2007.

Braconnot, P., Marzin, C., Grégoire, L., Mosquet, E., and Marti, O.: Monsoon response to changes in Earth's orbital parameters: comparisons between simulations of the Eemian and of the Holocene, Clim. Past, 4, 281–294, doi:10.5194/cp-4-281-2008, 2008.

CAPE: Last Interglacial Arctic warmth confirms polar amplification of climate change, Quaternary Sci. Rev., 25, 1383–1400, 2006.

Capron, E., Landais, A., Chappellaz, J., Schilt, A., Buiron, D., Dahl-Jensen, D., Johnsen, S. J., Jouzel, J., Lemieux-Dudon, B., Loulergue, L., Leuenberger, M., Masson-Delmotte, V., Meyer, H., Oerter, H., and Stenni, B.: Millennial and sub-millennial scale climatic variations recorded in polar ice cores over the last glacial period, Clim. Past, 6, 345–365, doi:10.5194/cp-6-345-2010, 2010a.

Capron, E., Landais, A., Lemieux-Dudon, B., Schilt, A., Masson-Delmotte, V., Buiron, D., Chappellaz, J., Dahl-Jensen, D., Johnsen, S., Leuenberger, M., Loulergue, L., and Oerter, H.: Synchronising EDML and NorthGRIP ice cores using $\delta^{18}O$ of atmospheric oxygen and CH_4 measurements over MIS5 (80–123 ka), Quarternary Sci. Rev., 29, 235–246, 2010b.

Clark, P. U. and Huybers, P.: Global change: Interglacial and future sea level, Nature, 462, 856–857, 2009.

Cuffey, K. M. and Clow, G. D.: Temperature, accumulation, and ice sheet elevation in central Greenland through the last deglacial transition, J. Geophys. Res.-Oceans, 102, 26383–26396, 1997.

Dahl-Jensen, D., Mosegaard, K., Gundestrup, N., Clow, G. D., Johnsen, S. J., Hansen, A. W., and Balling, N.: Past temperatures directly from the Greenland ice sheet, Science, 282, 268–271, 1998.

Dansgaard, W.: Stable isotopes in precipitation, Tellus, 16, 436–468, 1964.

Fichefet, T. and Maqueda, M. A. M.: Sensitivity of a global sea ice model to the treatment of ice thermodynamics and dynamics, J. Geophys. Res.-Oceans, 102, 12609–12646, 1997.

Fischer, N. and Jungclaus, J. H.: Effects of orbital forcing on atmosphere and ocean heat transports in Holocene and Eemian climate simulations with a comprehensive Earth system model, Clim. Past, 6, 155–168, doi:10.5194/cp-6-155-2010, 2010.

Gröger, M., Maier-Reimer, E., Mikolajewicz, U., Schurgers, G., Vizcaino, M. and Wingurth, A.: Changes in the hydrological cycle, ocean circulation and carbon/nutrient cycling during the last interglacial and glacial transitions, Paleoceanography, 22, PA4205, doi:10.1029/2006PA001375, 2007.

Hewitt, C. D. and Mitchell, J. F. B.: GCM simulations of the climate of 6 k BP: mean changes and inter-decadal variability, J. Climate, 9, 3505–3529, 1996.

Holden, P. B., Edwards, N. R., Wolff, E. W., Lang, N. J., Singarayer, J. S., Valdes, P. J., and Stocker, T. F.: Interhemispheric coupling, the West Antarctic Ice Sheet and warm Antarctic interglacials, Clim. Past, 6, 431–443, doi:10.5194/cp-6-431-2010, 2010.

Hourdin, F., Musat, I., Bony, S., Braconnot, P., Codron, F., Dufresne, J. L., Fairhead, L., Filiberti, M. A., Friedlingstein, P., Grandpeix, J. Y., Krinner, G., Levan, P., Li, Z. X., and Lott, F.: The LMDZ4 general circulation model: climate performance and sensitivity to parameterizations, Clim. Dynam., 27, 787–813, 2006.

Johnsen, S., Dansgaard, W., and White, J.: The origin of Arctic precipitation under present and glacial conditions, Tellus B, 41, 452–468, 1989.

Jouzel, J., Alley, R. B., Cuffey, K. M., Dansgaard, W., Grootes, P., Hoffmann, G., Johnsen, S. J., Koster, R. D., Peel, D., Shuman, C. A., Stievenard, M., Stuiver, M., and White, J.: Validity of the temperature reconstruction from water isotopes in ice cores, J. Geophys. Res., 102, 26471–26487, 1997.

Jouzel, J., Stiévenard, M., Johnsen, S. J., Landais, A., Masson-Delmotte, V., Sveinbjornsdottir, A., Vimeux, F., v. Grafenstein, U., and White, J. W. C.: The GRIP deuterium-excess record, Quaternary Sci. Rev., 26, 1–17, 2007.

Kageyama, M., Mignot, J., Swingedouw, D., Marzin, C., Alkama, R., and Marti, O.: Glacial climate sensitivity to different states of the Atlantic Meridional Overturning Circulation: results from the IPSL model, Clim. Past, 5, 551–570, doi:10.5194/cp-5-551-2009, 2009.

Kopp, R. E., Simons, F. J., Mitrovica, J. X., Maloof, A. C., and Oppenheimer, M.: Probabilistic assessment of sea level during the last interglacial stage, Nature, 462, 863–851, 2009.

Krinner, G., Genthon, C., and Jouzel, J.: GCM analysis of local influences on ice core δ signals, Geophys. Res. Lett., 24, 2825–2828, 1997.

Kurita, N.: Origin of Arctic water vapor during the ice-growth season, Geophys. Res. Lett., 38(2), L02709, doi:10.1029/2010GL046064, 2011.

Laepple, T., Werner, M., and Lohmann, G.: Synchronicity of Antarctic temperature and local solar insolation on orbital time scales, Nature, 471, 91–94, 2011.

Landais, A., Steffensen, J. P., Caillon, N., Jouzel, J., Masson-Delmotte, V., and Schwander, J.: Evidence for stratigraphic distortion in the Greenland Ice Core Project (GRIP) ice core during

Event 5e1 (120 kyr BP) from gas isotopes, J. Geophys. Res., 109, D06103, doi:10.1029/2003JD004193, 2004.

LeGrande, A. N. and Schmidt, G. A.: Sources of Holocene variability of oxygen isotopes in paleoclimate archives, Clim. Past, 5, 441–455, doi:10.5194/cp-5-441-2009, 2009.

Lourantou, A., Chappellaz, J., Barnola, J. M., Masson-Delmotte, V., and Raynaud, D.: Changes in atmospheric CO_2 and its carbon isotopic composition during the penultimate deglaciation, Quaternary Sci. Rev., 29, 1983–1992, 2010.

Madec, G. and Imbard, M.: A global ocean mesh to overcome the North Pole singularity, Clim. Dynam., 12, 381–388, 1996.

Marti, O., Braconnot, P., Dufresne, J. L., Bellier, J., Benshila, R., Bony, S., Brockmann, P., Cadule, P., Caubel, A., Codron, F., de Noblet, N., Denvil, S., Fairhead, L., Fichefet, T., Foujols, M. A., Friedlingstein, P., Goosse, H., Grandpeix, J. Y., Guilyardi, E., Hourdin, F., Idelkadi, A., Kageyama, M., Krinner, G., Levy, C., Madec, G., Mignot, J., Musat, I., Swingedouw, D., and Talandier, C.: Key features of the IPSL ocean atmosphere model and its sensitivity to atmospheric resolution, Clim. Dynam., 34, 1–26, 2010.

Masson-Delmotte, V., Jouzel, J., Landais, A., Stievenard, M., Johnsen, S. J., White, J. W. C., Sveinbjornsdottir, A., and Fuhrer, K.: Deuterium excess reveals millennial and orbital scale fluctuations of Greenland moisture origin, Science, 309, 118–121, 2005a.

Masson-Delmotte, V., Jouzel, J., Landais, A., Stievenard, M., Johnsen, S. J., White, J. W. C., Werner, M., Sveinbjornsdottir, A., and Fuhrer, K.: GRIP deuterium excess reveals rapid and orbital-scale changes in Greenland moisture origin, Science, 309, 118–121, 2005b.

Masson-Delmotte, V., Landais, A., Stievenard, M., Cattani, O., Falourd, S., Jouzel, J., Johnsen, S. J., Dahl-Jensen, D., Sveinsbjornsdottir, A., White, J. W. C., Popp, T., and Fischer, H.: Holocene climatic changes in Greenland : different deuterium excess signals at GRIP and NorthGRIP. J. Geophys. Res., 110, D14102, doi:10.1029/2004JD005575, 2005c.

Masson-Delmotte, V., Dreyfus, G., Braconnot, P., Johnsen, S., Jouzel, J., Kageyama, M., Landais, A., Loutre, M.-F., Nouet, J., Parrenin, F., Raynaud, D., Stenni, B., and Tuenter, E.: Past temperature reconstructions from deep ice cores: relevance for future climate change, Clim. Past, 2, 145–165, doi:10.5194/cp-2-145-2006, 2006a.

Masson-Delmotte, V., Kageyama, M., Braconnot, P., Charbit, S., Krinner, G., Ritz, C., Guilyardi, E., Jouzel, J., Abe-Ouchi, A., Crucifix, M., Gladstone, R. M., Hewitt, C. D., Kitoh, A., Legrande, A., Marti, O., Merkel, U., Motoi, T., Ohgaito, R., Otto-Bliesner, B., Peltier, R. W., Ross, I., Valdes, P., Vettoretti, G., Weber, S. L., and Wolk, F.: Past and future polar amplification of climate change: climate model intercomparisons and ice-core constraints, Clim. Dynam, 27, 437–440, doi:10.1007/s00382-005-0081-9, 2006b.

Masson-Delmotte, V., Stenni, B., Blunier, T., Cattani, O., Chappellaz, J., Cheng, H., Dreyfus, G., Edwards, R. L., Falourd, S., Govin, A., Kawamura, K., Johnsen, S. J., Jouzel, J., Landais, A., Lemieux-Dudon, B., Lourantou, A., Marshall, G., Minster, B., Mudelsee, M., Pol, K., Rothlisberger, R., Selmo, E., and Waelbroeck, C.: Abrupt change of Antarctic moisture origin at the end of Termination II, P. Natl. Acad. Sci. USA, 107, 12091–12094, 2010a.

Masson-Delmotte, V., Stenni, B., Pol, K., Braconnot, P., Cattani, O., Falourd, S., Kageyama, M., Jouzel, J., Landais, A., Minster, B., Barnola, J. M., Chappellaz, J., Krinner, G., Johnsen, S., Rothlisberger, R., Hansen, J., Mikolajewicz, U., and Otto-Bliesner, B.: EPICA Dome C record of glacial and interglacial intensities, Quaternary Sci. Rev., 29(, 113-128, 2010b.

NorthGRIP-community-members: High resolution climate record of the northern hemisphere reaching into last interglacial period, Nature, 431, 147–151, 2004.

Otto, J., Raddatz, T., and Claussen, M.: Strength of forest-albedo feedback in mid-Holocene climate simulations, Clim. Past Discuss., 7, 809–840, doi:10.5194/cpd-7-809-2011, 2011.

Otto-Bliesner, B. L., Marshall, S. J., Overpeck, J. T., Miller, G. H., Hu, A., and members, C.l.i.p.: Simulating Arctic climate warmth and icefield retreat in the last interglaciation, Science, 311, 1751–1753, 2006.

Polyak, L., Alley, R. B., Andrews, J. T., Brigham-Grette, J., Cronin, T. M., Darby, D. A., Dyke, A., Fitzpatrick, J. J., Funder, S., Holland, M., Jennings, A. E., Miller, G. H., O'Regan, M., Savelle, J., Serreze, M., St John, K., White, J. W. C., and Wolff, E.: History of sea ice in the Arctic, Quaternary Sci. Rev., 29, 1757–1778, 2010.

Rasmussen, S. O., Andersen, K. K., Svensson, A. M., Steffensen, J. P., Vinther, B. M., Clausen, H. B., Siggaard-Andersen, M.-L., Johnsen, S. J., Larsen, L. B., Dahl-Jensen, D., Bigler, M., Röthlisberger, R., Fischer, H., Goto-Azuma, K., Hansson, M. E., and Ruth, U.: A new Greenland ice core chronology for the last glacial termination, J. Geophys. Res., 111, D06102, doi:10.1029/2005JD006079, 2006.

Raynaud, D., Chappellaz, J., Ritz, C., and Martinerie, P.: Air content along the GRIP core: a record of surface climatic parameters and elevation in Central Greeland, J. Geophys. Res., 102, 26607–26613, 1997.

Rayner, N. A., Parker, D. E., Horton, E. B., Folland, C. K., Alexander, L. V., Rowell, D. P., Kent, E. C., and Kaplan, A.: Global analyses of sea surface temperature, sea ice, and night marine air temperature since the late nineteenth century, J. Geophys. Res.-Atmos., 108, 4407, doi:10.1029/2002JD002670, 2003.

Renssen, H., Seppa, H., Heiri, O., Roche, D. M., Goosse, H., and Fichefet, T.: The spatial and temporal complexity of the Holocene thermal maximum, Nat. Geosci., 2, 411–414, 2009.

Risi, C., Bony, S., Vimeux, F., Frankenberg, C., Noone, D., and Worden, J.: Understanding the Sahelian water budget through the isotopic composition of water vapor and precipitation, J. Geophys. Res., 115, D24110, doi:10.1029/2009JD013255, 2010a.

Risi, C., Bony, S., Vimeux, F., and Jouzel, J.: Water stable isotopes in the LMDZ4 general circulation model: model evaluation for present day and past climates and application to climatic interpretations in tropical isotopic records, J. Geophys. Res., 115, D24110, doi:10.1029/2009JD013255, 2010b.

Robinson, A., Calov, R., and Ganopolski, A.: Greenland ice sheet model parameters constrained using simulations of the Eemian Interglacial, Clim. Past, 7, 381–396, doi:10.5194/cp-7-381-2011, 2011.

Screen, J. A. and Simmonds, I.: The central role of diminishing sea ice in recent Arctic temperature amplification, Nature, 464, 1334–1337, 2010.

Severinghaus, J. P., Sowers, T., Brook, E., Alley, R. B., and Bender, M. L.: Timing of abrupt climate change at the end of the Younger Dryas interval from thermally fractionated gases in polar ice, Nature, 391, 141–146, 1998.

Shuman, C. A., Alley, R. B., Anandakrishnan, S., White, J. W. C., Grootes, P. M., and Stearns, C. R.: Temperature and accumulation at the Greenland Summit: Comparison of high-resolution isotope profiles and satellite passive microwave brightness temperature trends, J. Geophys. Res., 100, 9165–9177, 1995.

Sime, L. C., Tindall, J. C., Wolff, E. W., Connolley, W. M., and Valdes, P. J.: Antarctic isotopic thermometer during a CO_2 forced warming event, J. Geophys. Res., 113, D24119, doi:10.1029/2008JD010395, 2008.

Sime, L. C., Wolff, E. W., Oliver, K. I. C., and Tindall, J. C.: Evidence for warmer interglacials in East Antarctic ice cores, Nature, 462, 342–345, 2009.

Sjolte, J., Johnsen, S., Vinther, B. M., Masson-Delmotte, V., and Sturm, K.: Modeling the water isotopes in Greenland precipitation 1959–2001 with the meso-scale model REMOiso, J. Geophys. Res., 116, D18105, doi:10.1029/2010JD015287, 2011.

Steen-Larsen, H. C., Masson-Delmotte, V., Sjolte, J., Johnsen, S. J., Vinther, B. M., Bréon, F. M., Clausen, H. B., Dahl-Jensen, D., Falourd, S., Fettweis, X., Gallée, H., Jouzel, J., Kageyama, M., Lerche, H., Minster, B., Picard, G., Punge, H. J., Risi, C., Salas, D., Schwander, J., Steffen, K., Sveinbjörnsdóttir, A. E., Svensson, A., and White, J.: Understanding the climatic signal in the water stable isotope records from the NEEM shallow firn/ice cores in northwest Greenland, J. Geophys. Res., 116, D06108, doi:10.1029/2010JD014311, 2011.

Suwa, M., von Fischer, J. C., Bender, M. L., Landais, A., and Brook, E. J.: Chronology reconstruction for the disturbed bottom section of the GISP2 and the GRIP ice cores: implications for termination II in Grenland, J. Geophys. Res., 111, D02101, doi:10.1029/2005JD006032, 2006.

Svensson, A., Andersen, K. K., Bigler, M., Clausen, H. B., Dahl-Jensen, D., Davies, S. M., Johnsen, S. J., Muscheler, R., Parrenin, F., Rasmussen, S. O., Röthlisberger, R., Seierstad, I., Steffensen, J. P., and Vinther, B. M.: A 60 000 year Greenland stratigraphic ice core chronology, Clim. Past, 4, 47–57, doi:10.5194/cp-4-47-2008, 2008.

Swingedouw, D., Braconnot, P., and Marti, O.: Sensitivity of the Atlantic Meridional Overturning Circulation to the melting from northern glaciers in climate change experiments, Geophys. Res. Lett., 33, L07711, doi:10.1029/2006GL025765, 2006.

Swingedouw, D., Mignot, J., Braconnot, P., Mosquet, E., Kageyama, M., and Alkama, R.: Impact of Freshwater Release in the North Atlantic under Different Climate Conditions in an OAGCM, J. Climate, 22, 6377–6403, 2009.

Swingedouw, D., Delecluse, P., Guilyardi, E., and Marti, O.: The impact of global freshwater forcing on the thermohaline circulation: adjustment of North Atlantic convection sites in a CGCM, Clim. Dynam., 28, 291–305, 2007.

Turney, C. S. M. and Jones, R. T.: Does the Agulhas Current amplify global temperatures during super-interglacials?, J. Quaternary Sci., 25, 839–843, 2010.

Valcke, S.: OASIS3 User Guide, CERFACS, Toulouse, 2006.

Vinther, B. M., Buchardt, S. L., Clausen, H. B., Dahl-Jensen, D., Johnsen, S. J., Fischer, D. A., Koerner, R. M., Raynaud, D., Lipenkov, V., Andersen, K. K., Blunier, T., Rasmussen, S. O., Steffensen, J. P., and Svensson, A. M.: Holocene thinning of the Greenland ice sheet, Nature, 461, 385–388, 2009.

Waelbroeck, C., Labeyrie, L., Michel, E., Duplessy, J. C., McManus, J. F., Lambeck, K., Balbon, E., and Labracherie, M.: Sea-level and deep water temperature changes derived from benthic foraminifera isotopic records. Quaternary Sci. Rev., 21, 295–305, 2002.

Wagner, G., Laj, C., Beer, J., Kissel, C., Muscheler, R., Mazarik, J., and Synal, H. A.: Reconstruction of the paleoaccumulation rate of central Greenland during the last 75 kyr using the cosmogenic radionuclides ^{36}Cl and ^{10}Be and geomagnetic field intensity data, Earth Planet. Sc. Lett., 193, 515–521, 2001.

Werner, M., Mikolajewicz, U., Heimann, M., and Hoffmann, G.: Borehole versus isotope temperatures on Greenland: Seasonality does matter, Geophys. Res. Lett., 27, 723–726, 2000.

Yiou, F., Raisbeck, G. M., Baumgartner, S., Beer, J., Hammer, C., Johnsen, J., Jouzel, J., Kubik, P. W., Lestringuez, J., Stievenard, M., Suter, M., and Yiou, P.: Beryllium 10 in the Greenland Ice Core Project ice core at Summit Greenland, J. Geophys. Res., 102, 26783–26794, 1997.